

## Progress of the XFEL Project

### 1. Status of XFEL Construction

In FY2006, a five-year construction project of an 8-GeV XFEL facility was launched at SPring-8. This project was designated as one of the key technologies of national importance. Over the past three years, the construction has been progressing satisfactorily. Below we summarize our major achievements in 2008: (i) a large number of accelerator components were produced at factories; (ii) the manufacture of undulators was started; (iii) the specifications of XFEL beamline were determined; (iv) the electron-beam transport line from the 8-GeV linac to the SPring-8 storage ring was designed; and (v) the accelerator tunnel and undulator hall were completed.

Hereafter, we describe more details of the activities in XFEL construction. First, we have performed the reoptimization of accelerator parameters to provide a set of high-quality electron beams. To this purpose, we have performed start-to-end simulations from an electron gun to an 8-GeV beam dump. In these simulations, resistive wall wake fields in the undulator have been included. With these parameters, SASE-FEL radiation properties have been precisely evaluated. A summary of performance as well as the temporal profile are shown in Table 1 and Fig. 1, respectively.

To facilitate beam commissioning, we started to investigate beam commissioning-related subjects, i.e., the distribution of electron beam loss including dark current from the C-band acceleration system, the alignment-error tolerance of the accelerator structure, the effect of accelerator-structure vibration on beam quality, and the introduction of an rf deflector cavity for

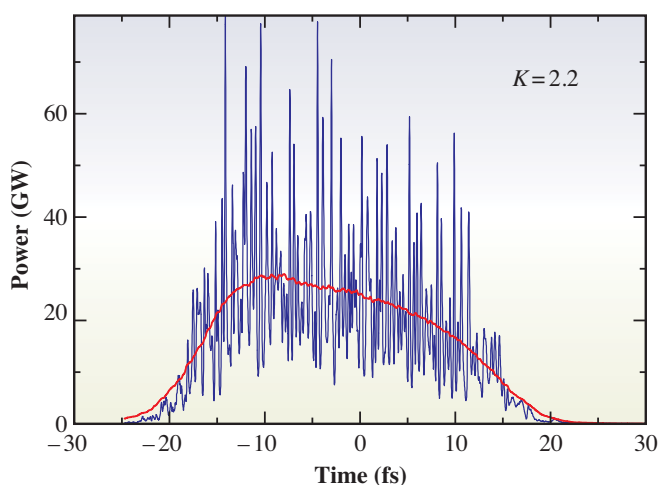


Fig. 1. Temporal profile of XFEL radiation at  $K=2.2$ . The red line shows a guide after smoothing.

Table 1. FEL radiation parameters at  $K=2.2$  (for fundamental radiation)

FEL parameter	$4.4 \times 10^{-4}$
Radiation wavelength (nm)	0.13
Photon energy (keV)	9.9
Bandwidth	$9.2 \times 10^{-4}$
Source size ( $\mu\text{m}$ , rms)	33
Angular divergence ( $\mu\text{rad}$ , rms)	0.73
Beam size @ sample position ( $\mu\text{m}$ , rms, 100 m from ID exit)	80
Peak power (GW)	29
Pulse energy (mJ/pls)	0.78
Photons per pulse (phs/pls)	$5.0 \times 10^{11}$
Pulse width (fs, FWHM)	30
Repetition rate (Hz)	60 (max) to 1 (min)
Power ratio of higher-order harmonic (2nd:1st)	$1.3 \times 10^{-4}$
Power ratio of higher-order harmonic (3rd:1st)	$2.8 \times 10^{-3}$



Fig. 2. Test bunker for high-power rf components.

measuring slice emittance and shot-by-shot longitudinal phase space.

A test bunker for high-power rf components was constructed in the SPring-8 site, as shown in Fig. 2, (i) to ensure the performance of the delivered rf components under a high-power condition, (ii) to establish an aging procedure for stable operation with design rf power and acceleration gradient and (iii) to accumulate fundamental data on dark current generation and aging period. The first high-power test was successfully performed: we confirmed to achieve a high acceleration gradient of 35 MV/m at a repetition rate of 60 Hz.

A new field correction procedure for an in-vacuum undulator was established with a manufactured prototype undulator in order to achieve the high field quality required for SASE XFEL. The new procedure

consists of the following steps; the conventional field correction is performed first to compensate phase and multipole-field errors in the field measurement bench with the vacuum vessel removed. To install the vacuum vessel, magnet arrays are detached from the mechanical frame and then built again inside it. The field distribution is then measured with the developed *in situ* field measurement system named SAFALI (self aligned field analyzer with laser instrumentation). A possible gap deformation during the above assembly process is analyzed with the measured phase error distribution and corrected by adjusting the ball screws supporting the magnet array assembly. Figure 3 shows the results of the new correction procedure. We found that the final phase errors in the new method are sufficiently suppressed down to the same level as that obtained in the bench with the vacuum vessel removed.

We achieved three progresses on the beam diagnostic system. First, a beam position monitor with a target resolution better than 1  $\mu\text{m}$  has been developed. The detection sensitivity to a transverse displacement (Fig. 4) has been evaluated. This result, combined with the measured noise-level of a new DAQ (data acquisition) system, shows that a resolution of 30 nm is possible. Second, a screen monitor has been developed for measuring a small beam profile of a few tens of micrometer scale. As shown in Fig. 5, we have distinguished a 2.5- $\mu\text{m}$  object. Third, two types of timing monitor system have been developed. One is a fast current transformer for the electron beam, and the other is an in-vacuum photodiode system for FEL radiation. Both the measurement systems have pulse responses of

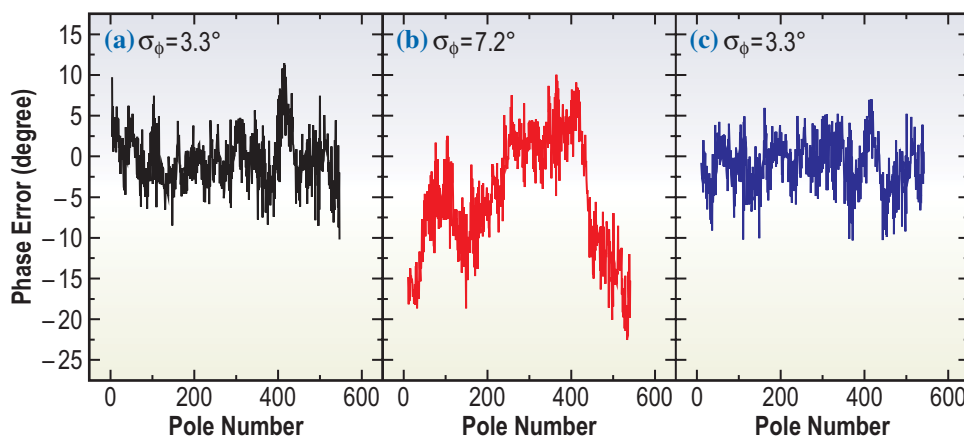


Fig. 3. Phase error distributions (a) before and (b) after reinstallation of magnet arrays and (c) after correction of gap deformation.

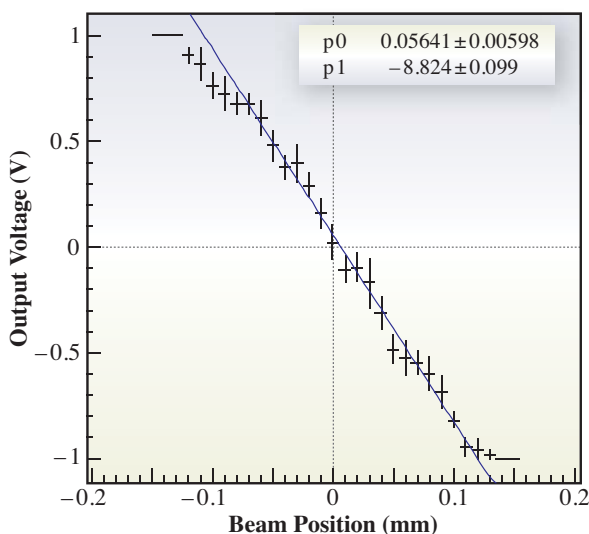


Fig. 4. Output voltages of beam position monitor measured at different beam positions.

~100 ps with an arrival timing accuracy of about 1 ps.

The R&D of LLRF (low level rf) and timing systems was carried out at the test accelerator. An electron beam time-jitter of about 46 fs in STD has been achieved at a position downstream of the C-band acceleration system. This result showed that the LLRF system almost satisfies the stability requirement for XFEL. To apply the developed systems in the XFEL accelerator on a scale of several hundred meters, an optical timing and reference rf signal transmission system using the WDM (wavelength division multiplex) method has been developed. The adopted WDM system using one optical fiber to transmit the rf signals generated by the master oscillator can handle five frequency signals corresponding to each multistage cavity

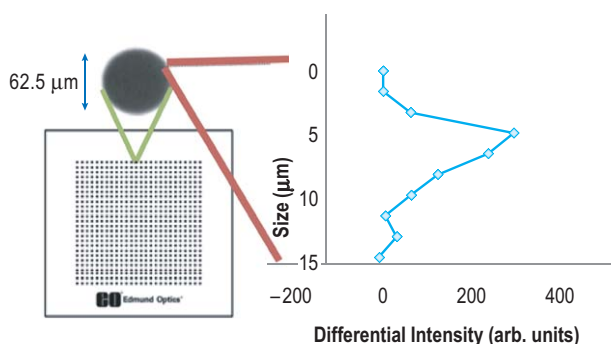


Fig. 5. Resolution of optical system of screen monitor. The dot diameter is 62.5 μm. The graph shows that the sharpness (resolution) of the dot edge is about 4 μm (FWHM). Edge sharpness is obtained by a differential operation of dot contrast.

acceleration unit for the velocity bunching. The experiment on optical signal transmission using an optical fiber of 500 m length revealed a very low noise characteristic of the system, as shown in Fig. 6, which never enhances the noise of the master oscillator through the transmission.

With respect to the R&D of vacuum technology, a laser beam welding procedure was established for a wide and square vacuum vessel that is used in a bunch compressor and a chicane where the energy-chirped electron beam becomes wider in the horizontal plane. A special rf contact for such a vessel was also developed to reduce impedance.

A remote-I/O card, called OPT-RMT i-DIO, was developed to realize a fast and precise control of a power supply for electromagnets even under a severe noise environment. High performance was confirmed by a test using an engineering sample of the OPT-RMT i-DIO and a prototype power supply. The developed FL-net test tool, which checks communication with a PLC, was tested in the rf test bunker. We found that the test tool is useful for debugging the configuration of a FL-net memory map. This will be used in a factory test before delivery to avoid a FL-net misconfiguration.

The XFEL facility can contain five photon beamlines. In 2008, the design work for the central beamline (BL3) has been completed. The beamline layout in the experimental hall as well as a detailed configuration are shown in Fig. 7 and Fig. 8, respectively. The main aim of this beamline is to manage hard X-ray FEL with a photon energy

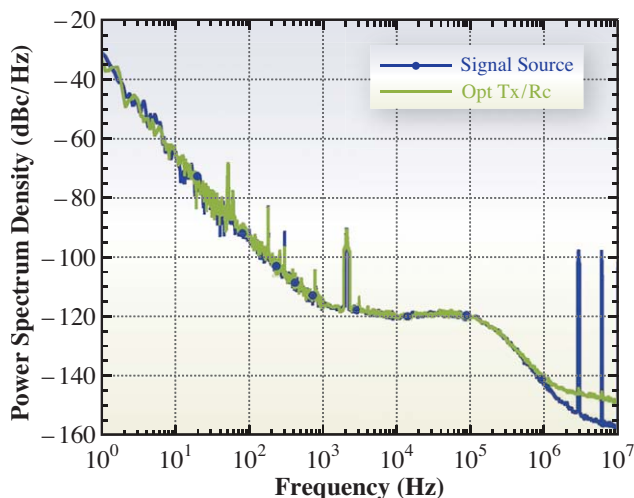


Fig. 6. Degradation of rf signal quality due to noise of optical rf signal transmission system. The increase in the level of noise at around 1 MHz corresponds to about 7 fs.

## XFEL

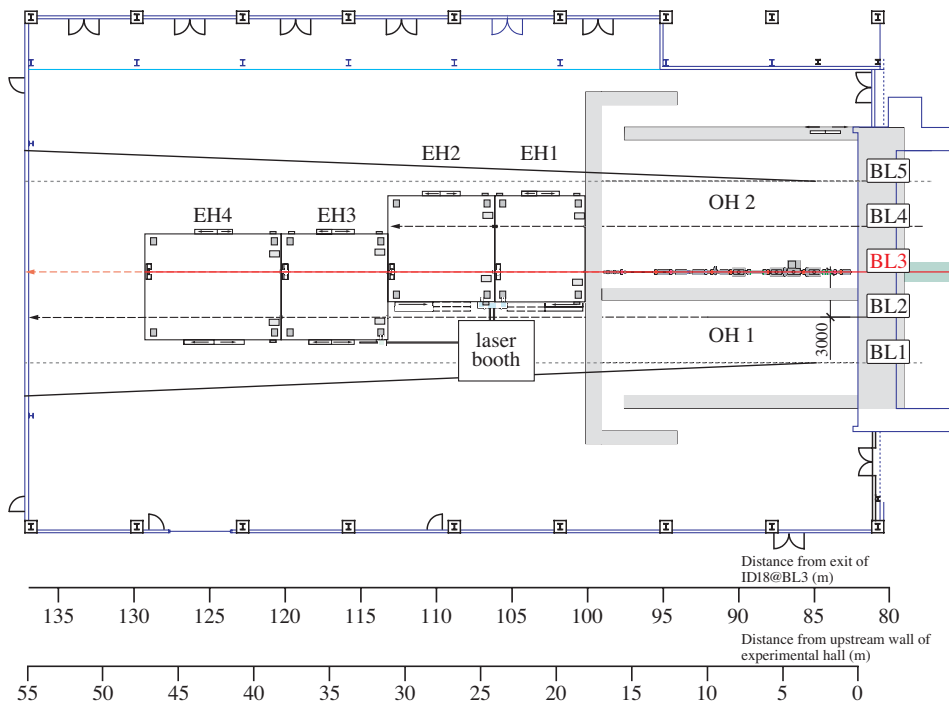


Fig. 7. Layout in experimental hall. Beamline optics are contained in the optics hutches, while experimental instruments are installed in experimental hutches. Synchronized lasers are set in the laser booth and distributed to experimental hutches.

above several keV; however, softer X-rays can be transported by adopting differential-pumping systems. A double-crystal monochromator and a pair of double-mirror systems are employed as principal beamline optics. The former delivers monochromatic X-rays in the range of 4 to 30 keV (with Si 111 diffraction), while the latter works as a low-pass filter below ~8 keV or ~15 keV. The beamline components are contained in

the optics hutch. Four experimental hutches for installing experimental instruments are set.

Most of foreseen XFEL experiments demands shot-by-shot measurement to cope with the instability inherent in the SASE process. To realize these experiments, a feasibility study of the dedicated data acquisition (DAQ) system has been started. Accordingly, the X-ray two-dimensional detector

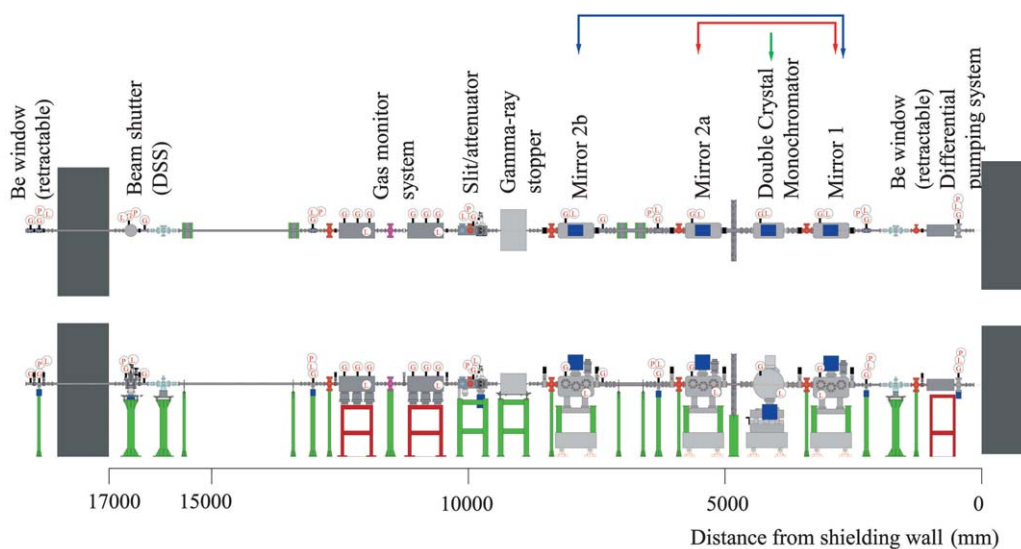


Fig. 8. Beamline configuration of BL3. A monochromator (green arrow), and a pair of mirrors 1 & 2a (red arrow) or 1 & 2b (blue arrow) are exclusively utilized as main optical components.

should record frame data at an XFEL repetition rate of 60 Hz with a high full-well capacity. The study including that of radiation damage has revealed the feasibility of the use of the direct detection charge-coupled device (CCD) in XFEL experiments, and yielded the concept of the multiport CCD sensor for XFEL. The finalized design has 64 readout ports with  $2k \times 2k$   $50 \mu\text{m}$  square pixels, and each pixel has a full-well capacity of 5 M electrons (Fig. 9).

The building construction has progressed on schedule. Figure 10 shows an aerial photograph of the construction site. The building frame and exterior finish were completed for both the accelerator and undulator buildings. The accelerator tunnel and undulator hall were made of radiation-shielding concrete walls whose thicknesses are 2 and 1.5 m, respectively. Soil improvement for the undulator building was carried out by a replacement method using crushed stones. A stable and high-density artificial rock bed with a maximum depth of 16 m was formed by rolling crushed stone layers at every 40 cm in depth, as shown in Fig. 11. The completion of both the accelerator and undulator buildings is scheduled in March 2009. A soil survey of the tunnel construction site for the beam transport line to the SPring-8 synchrotron was carried out in October 2008. This tunnel construction will be completed in March 2010.

## 2. Operation Status of SCSS Test Accelerator

The 250-MeV SCSS test accelerator was constructed in 2005 to perform basic R&D of the accelerator systems designed for 8-GeV XFEL. The first SASE FEL saturation was achieved in September 2007 (Fig. 12) [1]. Since May 2008, the extremely

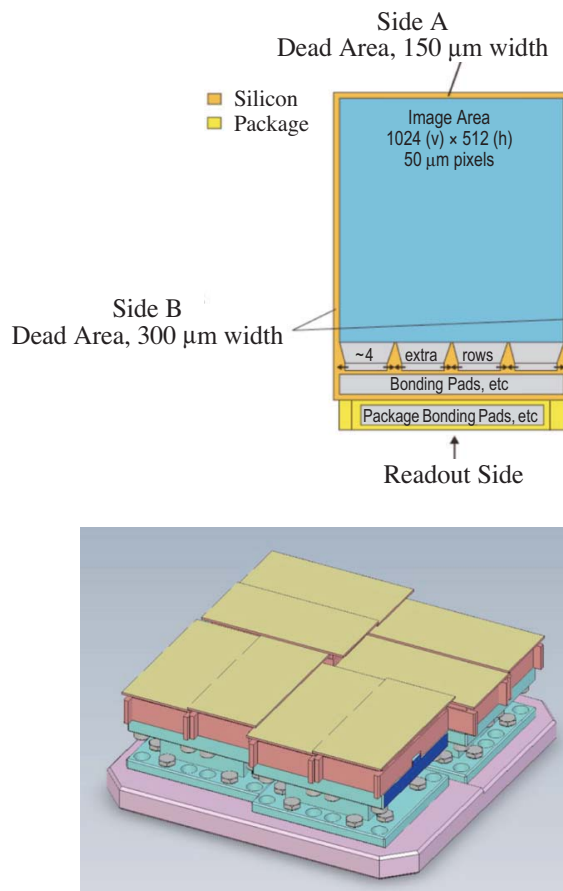


Fig. 9. Schematic sensor format of multiport charge-coupled devices (MP-CCDs) with eight readout nodes (left), and a tiled detector with a stepped array of eight devices with a total pixel number of  $2k \times 2k$  (right). Each readout node operating a 5 M pixel/sec readout rate enables synchronization to an XFEL repetition rate of 60 pps. The tiled detector has a through hole at the center whose size can be controlled by remote.



Fig. 10. Aerial photograph of XFEL construction site taken in November 2008.



Fig. 11. Rolling procedure for forming stable and high-density artificial rock bed.

intense FEL radiation in the EUV (extreme ultraviolet) region has been provided for users. User operation has been conducted over several months without any serious problems with the machine.

We introduce the R&D of accelerator components. A  $CeB_6$  cathode assembly, which had been stably used for about twenty thousands hours, was first replaced by a new one in January 2008. Figure 13 shows part of the exchange procedures in the accelerator tunnel and the old cathode just before being replaced. The cathode assembly was replaced without any serious problems. It took only one week including the processes of charging the voltage up to 500 kV and raising the temperature up to  $\sim 1800$  K. We could successfully reproduce the saturation of SASE FEL power with the new virgin cathode. This

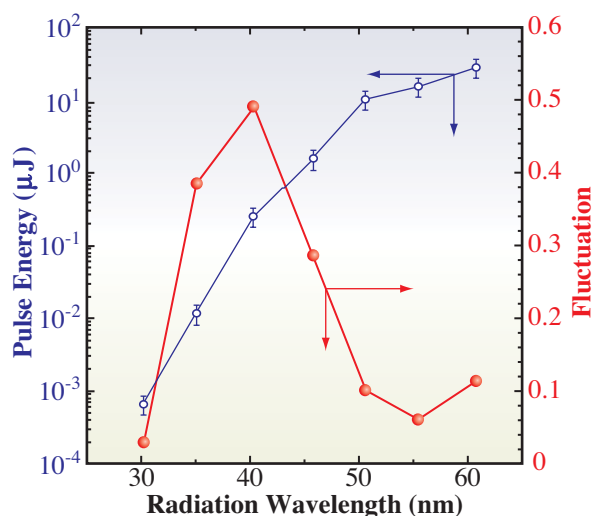


Fig. 12. Dependences of pulse energy and intensity fluctuation on radiation wavelength.

result verified the following issues: (i) the present design of the cathode assembly is suitable for quick and reliable exchange, (ii) the quality control of  $CeB_6$  single crystals is sufficiently high for SASE FEL reproducibility, and (iii) the beam tuning procedure after the cathode replacement is well established.

For the C-band acceleration system, the target performance was achieved in September 2008: a stable SASE FEL saturation has been confirmed with an acceleration gradient of 37 MV/m at a repetition rate of 60 Hz. The reliability of this high-gradient operation has been confirmed through a long-period operation over several months. Fault rate is kept small with an almost the same level as that in the low-gradient operation.

An event-synchronized data-acquisition system with a distributed shared-memory network has been installed and tested in the control system of the SCSS test accelerator. Fifty-four signals from the beam monitoring system such as current transformers, beam position monitors (BPM), and photodiode intensity monitors, have been successfully collected with 60 Hz

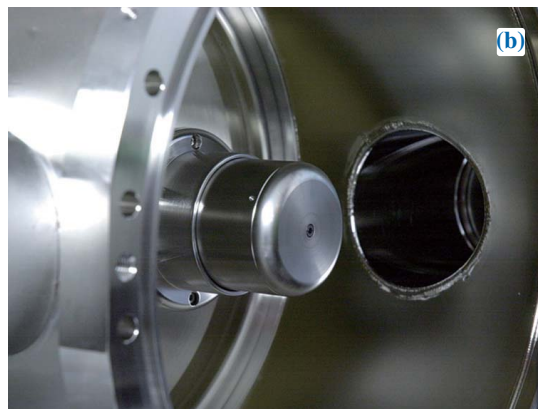


Fig. 13. One scene in cathode exchange procedures at  $CeB_6$  thermionic gun (a) and gun electrode with single-crystal  $CeB_6$  cathode just before the first replacement (b). The central dark part on the flat-shaped wehnelt is a  $CeB_6$  crystal.

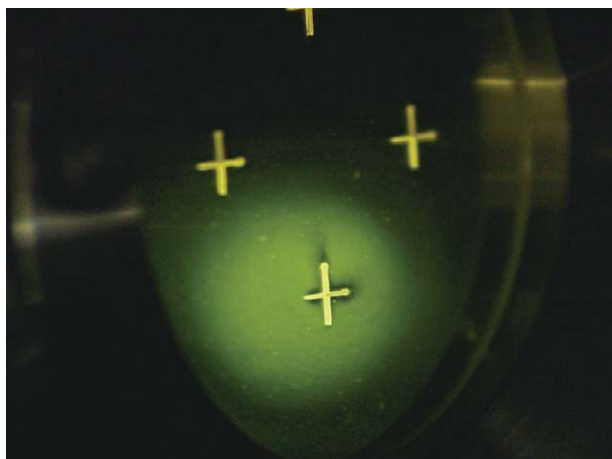


Fig. 14. Spatial profile of EUV radiation measured with YAG(Ce) crystal.

of beam operation cycles. The accumulated data are stored on a relational database for pulse-to-pulse correlation investigation. The BPM data have also been used for the effective correction of beam orbit and energy drifts.

After the first observation of the power saturation of FEL radiation, the accelerator parameters have been continuously optimized in order to improve FEL performance. This effort led us to achieve stable FEL radiation in the wavelength range between 50 to

60 nm during the user operation described below. Figure 14 shows the laser profile at the entrance of the experimental station.

Since the beginning of the user operation in May, we have conducted a user operation for 71 days for 10 user groups involving approximately 60 scientists including foreign researchers. The targets of the experiments are categorized into the following four groups: technical research preparatory for XFEL experiments; science with gas phase targets as atoms, molecules and clusters [2,3]; imaging and diffraction; and high-energy-density and warm matter.

In parallel with the user operation, we have continued to upgrade the EUV-FEL beamline. The plan is schematically shown in Fig. 15. The EUV-FEL can be delivered to four experimental stations at branches D, E, F and G, which is selected by a switching mirror. In 2008, we have developed branches B, D and E. In branch B, we have installed common diagnostics and optics such as a Ce:YAG fluorescent crystal to monitor beam profile, gas-filled attenuators to control pulse energy, nondestructive intensity monitors to measure pulse energy, and switching mirrors to steer the photon beam to branches D, E (G) and F. At the moment, an unfocused FEL beam can be steered to branches D and E. A focusing device will be installed in 2009.

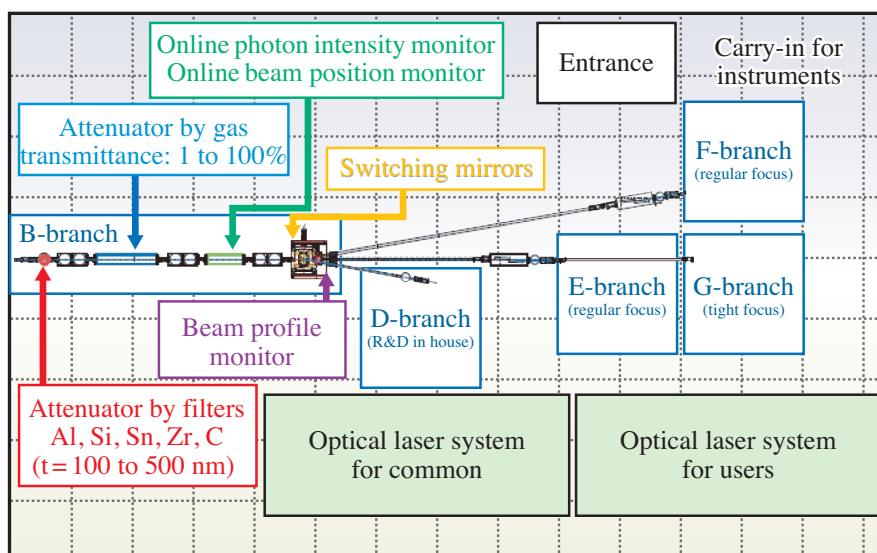


Fig. 15. Layout of EUV-FEL beamline.

References

- [1] T. Shintake *et al.*: Nature Photonics **2** (2008) 555.
- [2] T. Sato *et al.*: Appl. Phys. Lett. **92** (2008) 154103.
- [3] H. Fukuzawa *et al.*: Phys. Rev. A **79** (2009) 031201(R).